SOFT ROBOTICS
Volume 00, Number 00, 2019

DOI: 10.1089/soro.2018.0166

SoRo
Soft Robotics

Shape Memory Alloy-Based Soft Finger with Changeable Bending Length Using Targeted Variable Stiffness

Wei Wang,[1] Chak Yuk Yu,[2] Pablo Antonio Abrego Serrano,[2] and Sung-Hoon Ahn[2,3]

Abstract

This work described a bioinspired soft robotic finger with variable bending length to conform objects with different sizes by means of selectively varying the structural stiffness of its segments. The basic design is a shape memory alloy-based soft actuator with embedded stiffness-varying structures serving as modifiable endoskeletons. The stiffness-varying structure is composed of shape memory polymer (SMP) embedded with Nichrome (Ni-Cr) wires as heating elements. Joule heating of SMP through Ni-Cr wire inducing its phase change from the glassy state to the rubbery state enables the actuator structure change from the stiff state ($E = 125.65$ MPa) to the compliant state ($E = 3.33$ MPa). The Ni-Cr wire was designed with multiple solder tabs to enable the SMP that can be heated segmentally leading to the stiffness reduction of desired segments of finger to obtain different bendable lengths. A finger with three segments was fabricated, and its deformation and actuation force were measured based on different bendable lengths. A gripper was then assembled using two identical fingers where the angle between them can be manually adjusted. The angles for the two fingers with specific bending length were determined to enable them to form a closed configuration when maximum bending is reached. The grasping force of the gripper was then measured, and it was used to grip different objects. Results show that the performance of the gripper in gripping the size and weight of the object was markedly improved compared with the gripper that cannot vary its gripping length.

Keywords: soft robotics, soft gripper, shape memory materials, variable stiffness, variable length

Introduction

Soft organs in nature such as elephant trunk and octopus arm can vary their body's stiffness partially to generate motion and serve as a supporting structure concurrently or interchangeably.[1] The stiffness-varying capability enables them to interact effectively with the unconstructed natural environments; for instance, the elephant trunk can selectively soften or stiffen its different parts as a modifiable endoskeleton to conform objects with different sizes and transmit high forces attributed to its tightly packed muscle fibers arranged in different patterns (Fig. 1A). The role ascribed to the physical body for well interacting with the environments is called embodied intelligence indicating that a soft body is able to partly control deformations and movements by adapting and reacting to interaction forces.[2] Such capabilities of soft organs have inspired us to integrate soft technologies into robotic systems with bioinspired capabilities of compliance and adaptation for unconstructed environments. These soft robotic systems have shown significant advantages in the aspects of simplified mechanical and algorithmic complexity, adaptable morphology, diverse deformation, and low-cost fabrication, compared to their rigid counterparts.[3,4]

Soft robots especially soft manipulators have been demonstrated based on different actuation principles or smart materials, including shape memory alloy (SMA),[5,6] dielectric elastomer (DE),[7,8] soft pneumatic actuator,[9–11] and tendon-driven mechanism.[12,13] Among them, SMA based soft actuator is a relative optimum option to design soft manipulator in a small, compact, and lightweight configuration, because they only need small control circuits and batteries rather than the cumbersome accessories such as compressed air supply

[1]Department of Mechanical Engineering, Hanyang University, Seoul, Republic of Korea.
[2]Department of Mechanical and Aerospace Engineering, Seoul National University, Seoul, Republic of Korea.
[3]Institute of Advanced Machines and Design, Seoul National University, Seoul, Republic of Korea.

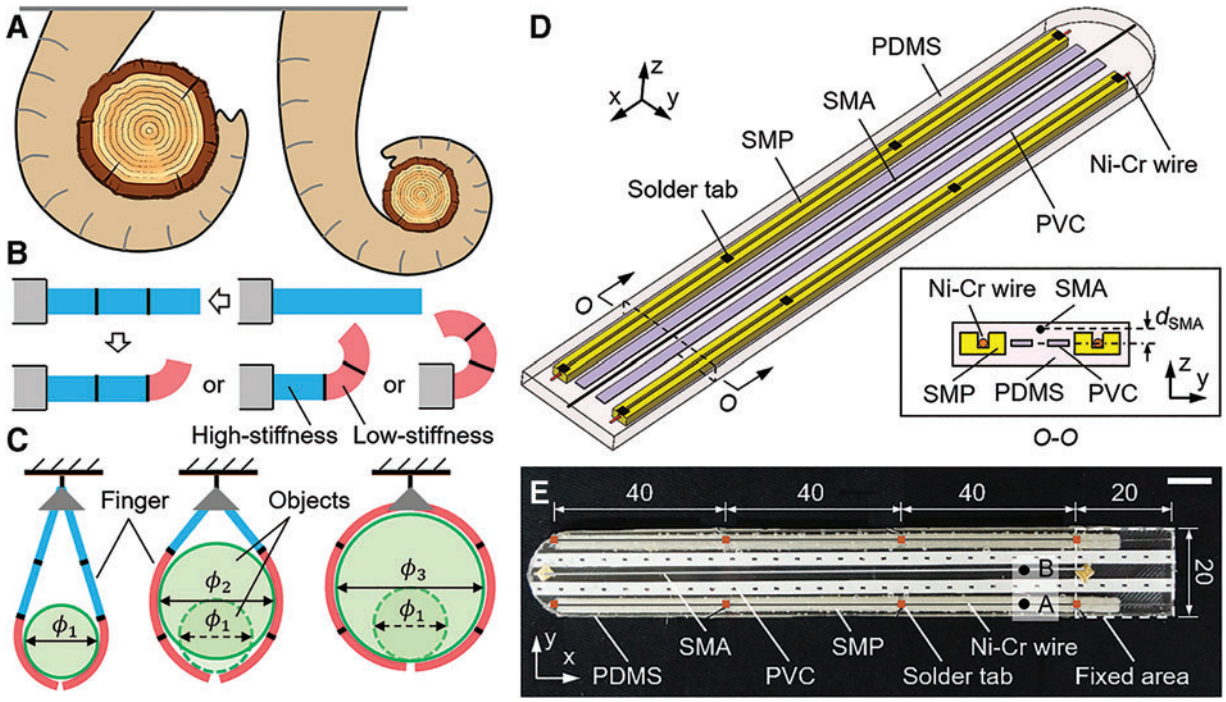

FIG. 1. Design and fabrication of soft finger. **(A)** Elephant trunk as a muscular hydrostat can selectively vary its segments' stiffness to conform objects with different sizes. **(B, C)** Schematic of a soft finger capable of reducing its structure stiffness to achieve changeable bending lengths with illustrational one, two, and three segments and grippers made up of them, respectively, with the largest object ($\phi_1 < \phi_2 < \phi_3$) that can be grabbed. *Short blue curves* indicate segments with high stiffness; short *red curves* indicate segments with low stiffness. **(D)** Schematic of the soft finger and its components. The *inset* shows the cross-section of the finger actuator indicating the relative positions of all components. **(E)** The *top view* of the fabricated soft finger actuator with all the components and all dimensions is in millimeters. Scale bar is 10 mm. Ni-Cr, Nichrome; PDMS, polydimethylsiloxane; PVC, polyvinyl chloride; SMA, shape memory alloy; SMP, shape memory polymer. Color images are available online.

for the pneumatic actuator, high-voltage power supply for the DE actuator, and motor for the tendon-driven mechanism. Previous studies on SMA based soft manipulators concentrated on how to improve their deformation or grasping force[5,6]; however, few contributions were made to control their compliance through achieving the adjustable structural configuration. Our previous work has demonstrated an SMA based soft hinged finger with the stiffness of only the designated local hinge segments being adjustable,[14] which further promotes us to design a soft finger with its entire structure being capable of varying its stiffness. Meanwhile, dividing the finger structure into several segments and controlling the stiffness of each segment individually enable the finger to achieve a changeable flexible length being capable of controlling localized or global deformations to adapt and react to external environments.

Variable stiffness mechanisms have been widely utilized for soft robots to achieve morphological shape change based on different principles. Antagonistic coupling of electroactive polymers was used to implement variable stiffness.[15] Flexible fluidic actuators were designed into variable stiffness multilayers.[16] Tendon-driven actuators can also be used to adjust structural stiffness.[17,18] Electro- and magnetorheological elastomers can only change stiffness in specific directions related to the applied external electric or magnetic field.[19,20] Material jamming as a variable stiffness approach has been widely used for designing both active and passive structures.[21–23] Some of the mentioned principles manifest that the stiffness change is coupled with their deformation, and it will be challenging for them to be designed as versatile stiffness-change structures with passively adaptive capability. In contrast, working mechanisms being concomitant with the bulky accessories have built up many obstacles to be designed as an independent robotic system with compact configuration. Materials featuring a low melting or phase change temperature can be rapidly obtained by a stiffness reduction with high thermal input, but the stiffness restoring always requires a long time for cooling.[14,24,25] However, this principle can be easily integrated with soft actuators and structures in a compact configuration.[26–28]

Inspired by the elephant trunk, this work aims to design a soft finger capable of varying its entire stiffness between the high state and the low state by means of embedded stiffness-varying materials serving as modifiable endoskeletons. Dividing the actuator into segments and selectively reducing the segments' stiffness enable the finger to achieve a changeable bending length where the bending deformation concentrates on the segments with low stiffness (Fig. 1B). Two fingers are then assembled together to form a gripper with adjustable bending length to enhance its grasping capability when grasping objects with different sizes (Fig. 1C). The basic design is a SMA based soft finger with embedded stiffness-varying structure, which is composed of shape memory polymer (SMP) embedded with Nichrome (Ni-Cr) wires as

heating elements. The Ni-Cr wire was designed with multiple solder tabs to enable the SMP to be heated segmentally, changing its phase from the glassy state with high stiffness to the rubbery state with low stiffness, which can result in the stiffness reduction of the finger's targeted segments enabling it to have different effective bendable lengths. A finger with three segments was fabricated, and its deformation and actuation force were measured based on different bendable lengths. A gripper was then assembled using two identical fingers where the included angle between them can be manually adjustable. The gripper's grasping performance was evaluated, and the result showed that the grasping performance in gripping the size and weight of the object was markedly improved compared to the gripper without varying ability.

Design and Fabrication

The basic design used in this study is a self-actuating SMA based soft actuator with variable stiffness being capable of achieving targeted bending deformation. The schematic of the soft finger and all its components are described in Figure 1D. The finger actuator contains smart material, stiffness changeable material, heating element, a flexible polymeric matrix, and embedded flexible reinforcement. In this study, we used SMA (55 wt% Ni, 45 wt% Ti, Flexinol; Dynalloy) wire as the smart material for actuation, SMP (MM5520; SMP Technologies) as the stiffness changeable material, Ni-Cr (80 wt% Ni, 20 wt% Cr) wires as the heating element, polyvinyl chloride (PVC) plate as the flexible reinforcement, and polydimethylsiloxane (PDMS, Sylgard 184; Dow Corning) elastomer as the flexible matrix. All the materials used are commercially available, and their main properties are listed in Supplementary Table S1.

The SMP structure was fabricated by three-dimensional (3D) printing with a groove across the whole length for mounting the Ni-Cr wire. Multiple solder tabs were designed to attach on the Ni-Cr wire such that the wire can be heated segmentally by applying the electric current between every two different solder tabs. The more solder tabs, the more segments can be selected, and the stiffness of a wider range of finger positions can be controlled. Hence, the actuator can achieve the targeted stiffness variation through Joule heating corresponded segments of SMP using the Ni-Cr wire embedded in SMP.[29–31]

With the temperature below its glass transition temperature (T_g), SMP is in the glassy state with high modulus, corresponding to the actuator section in the high stiffness state; above the T_g, SMP markedly softened and transited to the rubbery state with low modulus, corresponding to the actuator section in the low stiffness state. With targeted segments in the low stiffness, applying an electric current to the SMA wire to increase its temperature through Joule heating until its austenite phase transition temperature can enable the SMA wire located off-middle plane to contract in the matrix to generate the bending deformation over the segments in the low stiffness state.[32,33] Besides, two PVC plates cut into rectangular shape were symmetrically embedded in PDMS to enhance modulus of the entire structure to prevent the structure from being compressed and to allow the finger to obtain a faster recovery.[34,35]

Each finger actuator was fabricated by first building an acrylonitrile butadiene styrene (ABS) mold using a 3D printer (200 DP; Sindorin) in the shape of the finger with slots and holes for positioning all the embedded components. One SMA wire was prestrained and placed with a fixed off-middle plane distance of d_{SMA} of 1 mm for unidirectional bending actuation. The SMP structure with dimensions of $130 \times 3 \times 1.7$ (mm, length × width × thickness) was fabricated using the same 3D printer with a groove at the center. In this study, the Ni-Cr wire with a diameter of 0.15 mm was divided into three segments with four uniformly distributed solder tabs in the length of 40 mm for each segment. The Ni-Cr wire was first placed in the groove of the SMP, and then two of these integrated structures are placed symmetrically in the actuator mold in parallel to the SMA wires. The relative positions of SMA and SMP are shown in the schematic of the cross-section of the actuator in the inset of Figure 1A. Besides, the PVC plate cut into the designed pieces by a laser cutter (M-300; Universal Laser Systems) was also placed in the mold. After assembling, a PDMS solution with a weight ratio of 10:1 monomer to hardener was poured into the mold for curing at a temperature of 50°C for 6 h. The finger actuator as shown in Figure 1D can be finally obtained by removing the ABS mold, and its overall dimensions are $145 \times 20 \times 3$ (mm, length × width × thickness) with a fixed end of 20 mm in length.

Results and Discussion

Variable stiffness of finger structure

The change of elastic modulus of SMP on a temperature scale is schematically described in the inset of Figure 2A. The elastic modulus of SMP decreases by three orders of magnitude when they change from the glassy state to the rubbery state upon heating above its T_g.[36] The finger is capable of tuning its structure stiffness locally by selectively softening the targeted segments of the embedded SMP structure using Ni-Cr wire. The electric current was applied to the Ni-Cr wire for heating the SMP to the temperature above its T_g to change it from the glassy state to the rubbery state, which leads to the significant decrease in stiffness of the finger structure. The reduced stiffness can be restored after free cooling the heated SMP until its temperature reaches below its T_g.

The Ni-Cr wire was applied with the electric current of 1.0 A (with power consumption of 0.062 W/mm) to determine the heating and cooling time for switching the stiffness of the finger structure between a high state and a low state. A thermal camera (CX-320U; Hanmac) was used to detect the temperature change of the positions of SMP and SMA (point A and point B, Fig. 1E and middle inset of Fig. 2A) in real time, and the result is shown in Figure 2A. It can be seen that the temperature of SMP increases rapidly and it takes around 15 s to achieve its T_g of 55°C. In this work, the SMP was heated above 60°C using about 20 s to ensure the whole SMP structure can be changed entirely to rubbery phase, and a cooling time of 75 s was required to reduce the SMP's temperature below 40°C to ensure the SMP has been changed back to the glassy phase. Moreover, after heating the embedded SMP for 20 s, an experimentally obtained lower electric current of 0.5 A (0.031 W/mm) was needed to maintain the SMP in the low-stiffness state (Fig. 2A). It is notable that the temperature of the SMA position (point B) is always lower than the A_s of SMA during all heating processes

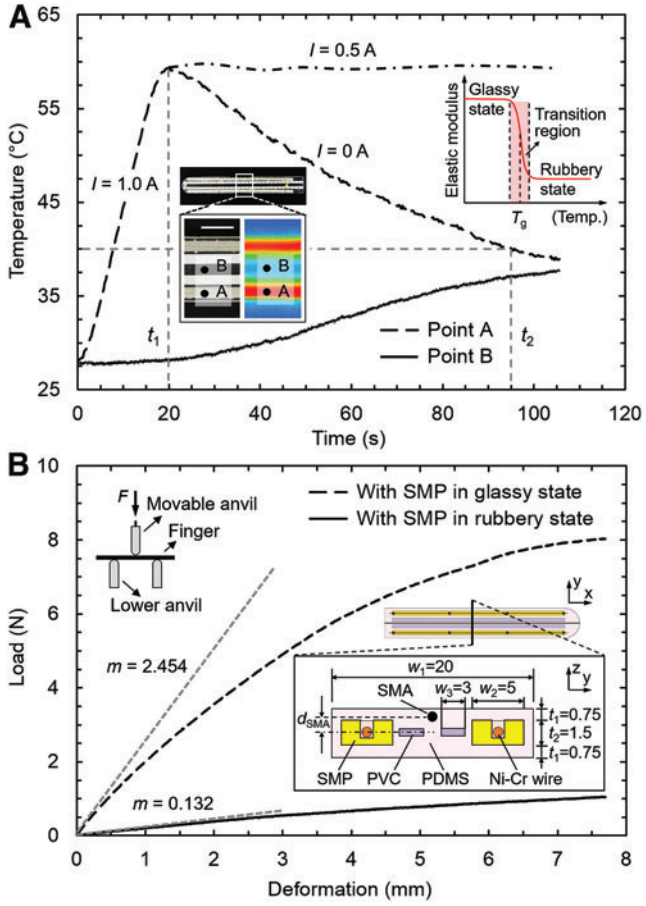

FIG. 2. Variable stiffness of finger structure. **(A)** Temperature variation of SMP and SMA by heating the SMP from the beginning to time t_1 and then cooling the SMP from time t_1 until time t_2 or maintaining the temperature SMP at around 60°C by continuously inputting an electric current of 0.5 A. The *insets* show the schematic of SMP modulus' change on a temperature scale and the fabricated finger with its thermal image during the heating process. **(B)** Results of the three-point bending test (*top-left inset*) of the finger structure with embedded SMP in the rubbery state and in the glassy state. The *inset* shows the schematic and geometric dimension of the cross section of the finger structure, and all dimensions are in millimeters. All scale bars are 10 mm. Color images are available online.

of the SMP indicating that there is no thermally caused strain of SMA wire through the SMP's heating process.

The stiffness of the actuator can be considered as the sum of the stiffness of all embedded components. The schematic of the actuator structure and its geometric parameter of the cross-section area are described in the inset of Figure 2B. Then, the bending rigidity of the actuator structure can be given and calculated by the sum of bending rigidity of PDMS matrix, SMA wire, Ni-Cr wires, and SMP and PVC structures (see Supplementary Data). The actuator in low and high stiffness was determined by the embedded SMP structures with a glassy modulus of ~800 MPa and a rubbery modulus of ~1.4 MPa,[37] respectively. The bending modulus of the actuator with fixed geometrical dimensions was calculated as 122.25 and 3.36 MPa in high and low stiffness states. Both the bending modulus of the actuator in low and high stiffness states were also measured using a three-point bending method (ASTM D 790-03) through a universal testing machine (5948; Instron) with a three-point flexure fixture (2810-400; Instron). The results are illustrated in Figure 2B, and $E_A = L^3 m/[4w_1(2t_1 + t_2)^3]$ of the actuator structure can be calculated, where m is the gradient of the load-displacement curve (2.454 for high-stiffness state and 0.132 for low-stiffness state), as 125.65 MPa in the high stiffness and 3.33 MPa in the low stiffness, which correspond to a ratio of ~38 times. Comparing theoretical and experimental results, the theoretical calculation is able to predict the actuator stiffness in the two different states. However, there are still some differences (mean error 2.7% and 1.0%), which could be due to the fabrication and position errors of the structural components. It should be noticed that the stiffness change can be tailored by modifying the geometrical parameters of the embedded SMP structures.

Deformed configurations of finger actuator

Each segment of the finger actuator can individually change its stiffness from the high state to the low state by heating the embedded SMP structure's corresponding segments above its T_g. That is, first the stiffness of the finger segments is selectively reduced with an applied electric current of 1.0 A on SMP (actually is Ni-Cr wire) for 20 s, and then the targeted finger segments in low stiffness are maintained with a continuously applied lower electric current of 0.5 A on SMP; afterward, keeping the finger segments in low stiffness, actuating the embedded SMA wire with the length of 120 mm by applying the electric current of 0.6 A (~0.020 W/mm) can achieve the finger's targeted bending deformation through Joule heating to reach its A_s; the eccentrically positioned SMA contracts in the PDMS matrix to produce a bending moment resulting in the bending deformation concentrated on segments with low stiffness and the whole process take around 5 s; and un-actuating SMA will enable the finger to recover its original shapes; finally the continuously applied electric current of 0.5 A on SMP can be removed, and the stiffness of the finger will change back from the low state to the high state.

A finger actuator with three segments can provide eight different configurations by deforming different amounts of segments (none, one segment, two segments, and three segments) as shown in Figure 3. In the figure, an array with three sequential numbers is used to indicate the stiffness state of one actuator with three segments where "0" represents the corresponding segment with low stiffness, and "1" represents the corresponding segment with high stiffness. The insets in each figure show the schematic of bending deformation and the thermal image of the finger actuator where the bright red areas indicate that the segments with embedded SMP are heated for the low-stiffness state and dash lines indicate the actuator profile.

Evaluation of actuation deformation and force

The bending deformation of the finger with one, two, and three segments (Fig. 3B, E, H) was measured, respectively. The geometric shape of the bending section was approximated by a circular arc during actuation, and the corresponding central angle was considered as the bending angle (Supplementary Fig. S1). The previous study has explored that the maximum bending curvature of the SMA based soft

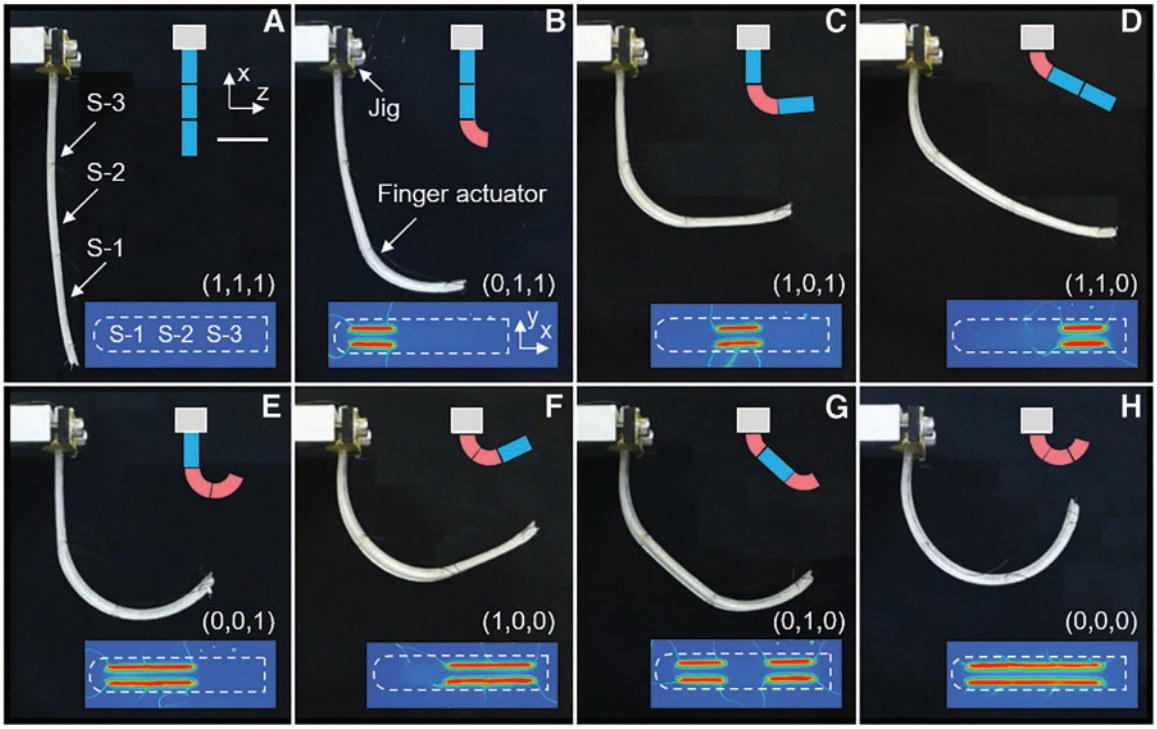

FIG. 3. The different configurations achieved by one finger actuator. **(A)** The original straight configuration of the finger actuator with three segments. Finger actuator with one bending segment **(B–D)**, two bending segments **(E–G)**, and three bending segments **(H)**, respectively. The *insets* in each figure show the schematic deformation and the corresponding thermal image of the finger actuator. Scale bar is 20 mm. Color images are available online.

actuator is determined by the total length of the flexible segments regardless of their position.[5] According to the developed mechanical model based on the Brinson modeling of SMA (see Supplementary Data),[5,38,39] the maximum bending angle of the finger structure in this study with one, two, and three segments in low stiffness state was calculated as 74.23°, 144.24° (72.12° per segment), and 206.32° (68.77° per segment), respectively. The corresponding experimental deformation was measured as 70.15°, 135.12° (67.56° per segment), and 195.05° (65.02° per segment). Both the experimental and modeling results of the maximum bending angle of the finger structure with different bendable segments are illustrated in Figure 4A. The contracting length of embedded SMA wire in both rigid and flexible segments will be

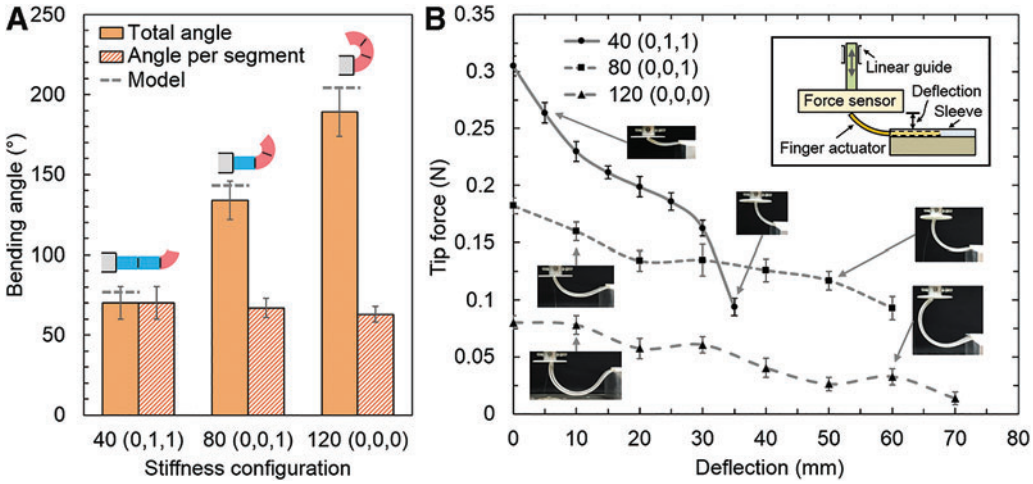

FIG. 4. The bending deformation and actuation force of the finger actuator. **(A)** Comparison of experimental and modeling results for finger actuator with a different number of flexible segments. The *insets* show the schematic of the bent finger actuator. **(B)** Measurements of the actuation force of finger actuator with different deflective deformations as shown in the corresponding *insets*. The *upper-right inset* shows the actuation force experimental setup. Scale bar is 20 mm. Color images are available online.

concentrated on the flexible segment leading to a larger bending angle per segment, with a smaller number of segments. The total bending angle is getting larger with the increase in segment number. The mechanical model can predict well for the maximum bending deformation, yet there are still some differences between the experimental results and modeling data, which are mainly due to the effect of gravity during measurements and the actuator fabrication errors.

The deformation recovery performance of a 120-mm actuator was also tested by repeatedly actuating and un-actuating the actuator for 100 times according to the actuation method in Deformed Configurations of Finger Actuator section. The measured results show the configurations of the bending actuator before the first actuation with an initial bending angle of 10.63°, during the actuation with an averaged maximum bending angle of 195.09° and after 100-times actuation with a residual angle of 23.59°. The final residual deformation amount for the 120-mm actuator can be calculated as 6.67%, which means 2.22% for each segment with length of 40 mm (Supplementary Fig. S2). It can be seen that the actuator can perform a good shape recovery which can be further improved by adding one more antagonistically actuated SMA wire or improving the elasticity of the actuator structure.[35,40]

The actuation force of the bending finger actuator was measured using a dynamometer (9256C2; Kistler). The stiff part of the finger actuator was inserted to a sleeve fixed on a platform, and the dynamometer was installed to a linear guide, as shown in the top-right inset of Figure 4B. The experiments were conducted for tip deflections varying from 0 mm to maximum touchable height by adjusting the height of the dynamometer incrementally. When actuating the SMA wires embedded in the soft finger, the force generated by the fingertip with different softening segments of the finger structure in the vertical direction was measured and shown in Figure 4B. It can be seen that the finger actuator with a shorter flexible length can generate a smaller deflective deformation but a larger tip force. Meanwhile, with the increase in fingertip deflection, the force generated by the fingertip dropped rapidly for the finger actuator with one bending segment and almost linearly for the actuator with both two and three bending segments. That is because the inherent softness of the finger structure generates shape distortion when encountering blocking force and a longer flexible length results in more distortion.

Evaluation of grasping performance

Experimental results on actuation deformation and force indicate that the finger actuator with a shorter flexible length can generate a smaller deflective deformation but a larger tip force; inversely, the finger actuator with a longer flexible length can generate a larger deflective deformation but a smaller tip force. These results inspired our design of soft gripper with obtainable different configurations where the fingers with shorter bendable length can be utilized to grip smaller but heavier objects and longer bendable length can be utilized to grip larger but lighter objects. Two identical fingers with obtainable one, two, and three flexible segments were assembled symmetrically to form a plane gripper where the two fingers always generate identical deformation (Fig. 3B, E, H) throughout all measurements. The robotic finger was first inserted in a sleeve with a fixed length of 20 mm, and then two fingers were mounted to a metacarpal using revolute joints as shown in Figure 5A. Because of revolute joints, the included angle between two fingers can be manually adjusted when the fingers have different flexible segments. The included angle was determined to enable the gripper to achieve a closed state with two fingertips just contacting each other when the composed fingers achieved their maximum bending deformation. The finger used for assembling the gripper was determined to have one, two, and three flexible segments with stiffness states of the three segments represented as (0,1,1), (0,0,1), and (0,0,0), respectively. As shown in Figure 5B, the corresponding included angles between two fingers were experimentally determined as 24°, 80°, and 100°, respectively. Based on the different included angles, the object with the maximum size and weight can be gripped by the gripper which will also be different.

To evaluate the grasping force, the gripper was installed to the same universal testing machine (5948; Instron) to measure the force generated by the gripper on fixed cylindrical objects with different diameters from caging the objects to their separation. The cylinder objects were designed with a diameter ranging from 20 mm to the maximum size that can be caged by the gripper. The two SMA wires embedded in the two fingers were connected in series and were actuated simultaneously using an electrical current of 0.60 A regardless of the target objects. The vertical maximum pulling forces generated by the gripper with the mentioned three different configurations on the fixed objects are shown in Figure 5C. There is an optimal point to achieve the maximum pulling force for the gripper in each configuration as the maximum grasping force is mainly determined by the largest passively available contacting area between the object and fingers during each grasping process. It can be observed from experiments that the largest achievable contacting area increases first and then decreases, along with the increasing size of cylindrical objects, as described in bottom inset of Figure 5C where the finger with two flexible segments was used to gripping different cylindrical objects (diameter is 40, 60, 80, and 100 mm, respectively) with the contacting areas between fingers and the object highlighted in yellow.

The maximum grasping forces (corresponding to the diameter of the cylindrical object) obtained by the gripper in three different configurations with fingers having one, two, and three flexible segments are 1.79 N (30 mm), 1.38 N (80 mm), and 1.30 N (90 mm), respectively. The maximum force for each configuration is getting smaller, which is mainly because the finger with a longer flexible length will generate smaller actuation force as measured in the previous experiment. Moreover, the grasping capability of the gripper with changeable configuration is represented by the purple region, which is the union of the areas under the three curves of pulling force plotted against the size of the object showing the grasping ranges of the gripper in the three configurations (Fig. 5C). To sum up, the gripper's performance in gripping the size and weight of the object was markedly improved compared with the gripper with a fixed configuration. To verify the gripper's performance (Fig. 5D–G and Supplementary Movie S1), the gripper with one flexible segment is used to grip cylindrical objects with diameter of 30 mm (with its weight of 1.55 N) and 50 mm (0.81 N), and the gripper

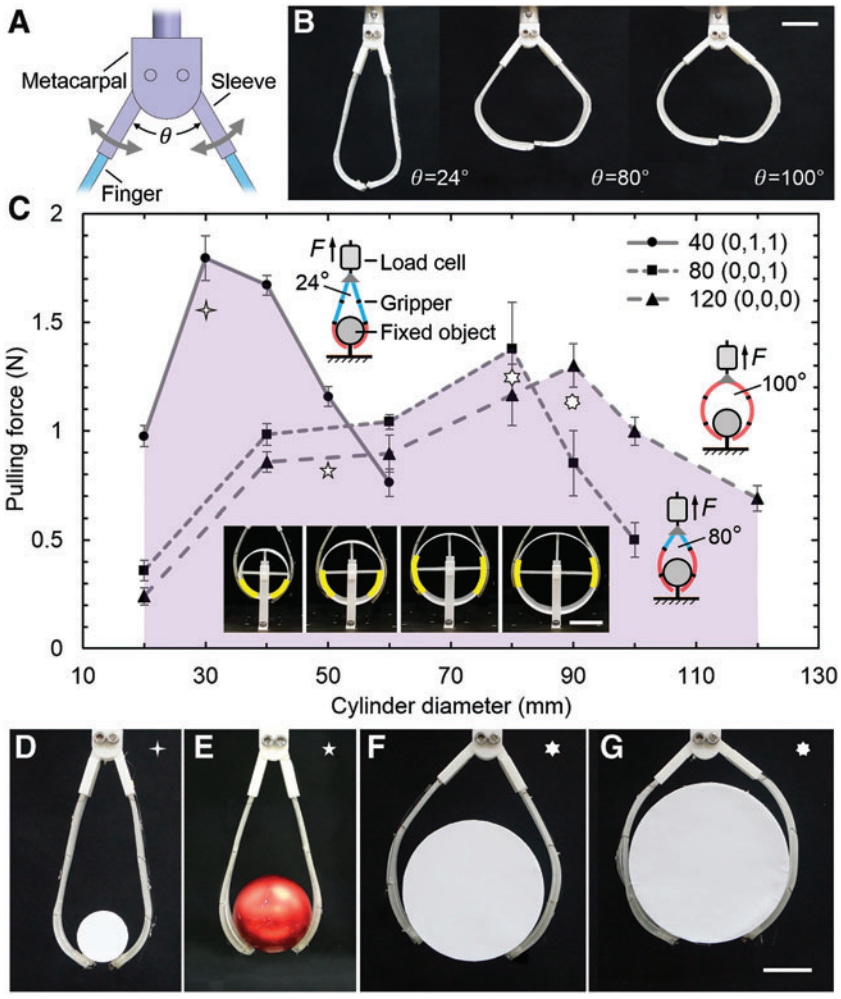

FIG. 5. Assembled gripper and its grasping performance. **(A)** Schematic of the assembled gripper. **(B)** The three configurations of the gripper with included angles between two fingers were determined as 24°, 80°, and 100° to enable the gripper to have a closed state when the composed fingers achieved their maximum bending deformation. **(C)** Grasping force of the gripper with one, two, and three flexible segments from caging different cylindrical objects to their separation, respectively. The *insets* show the schematic of experimental setups for measuring gripping force and gripper with composed fingers with two flexible segments gripping different cylindrical objects. **(D–G)** The gripper with different flexible lengths is used to grip cylindrical objects with different sizes and weights. The corresponding locations of the objects are also marked in **(B)**. All scale bars are 30 mm. Color images are available online.

with two and three segments is used to grip cylindrical objects with diameters of 80 mm (1.25 N) and 90 mm (1.12 N), respectively.

Conclusions

Compared with our previous work on an SMA based soft hinge actuator with localized variable stiffness,[14] this study inspired by the elephant trunk described a soft finger with its entire structure being capable of varying its stiffness by means of embedded variable stiffness structures serving as a modifiable endoskeleton. Meanwhile, dividing the finger structure into several segments and through reducing the stiffness of the target segments, the finger can achieve a changeable bending length to adapt and react to external environments.

The variable stiffness of the actuator was achieved by embedding the phase-changing materials in the actuator's matrix. The bending modulus of the actuator with stiffness in the high state and in the low state was measured as 125.65 and 3.33 MPa, respectively, corresponding to around 38-fold variations in stiffness. The actuator with an applied electrical current of 1.0 A to the SMP structure needed 20 s to change its stiffness from the high state to the low state, and the inverse process without the need of applying electrical current needed 75 s through free cooling. After the finger reached its low stiffness state, a lower current of 0.5 A was required to maintain the SMP in rubbery state, under which situation the SMA can be actuated to bend the finger for grasping. Besides, the required 75 s for the stiffness change in the inverse process are not involved for working state but for configuration transition to achieve different flexible lengths, and no extra power consumption is required to maintain the shape in high stiffness state.

A soft finger with three segments can change their stiffness individually enabling the finger to have different effective bending lengths. Two identical fingers were then constructed as a gripper with the manually adjustable included angle. The gripper was manually set as different included angles of 24°, 80°, and 100° between the two fingers with each finger having one, two, and three bendable segments. The grasping force of the gripper was measured, and grasping performance was verified by gripping different objects. Results show that the gripper's performance on gripping various sizes and weights was markedly improved compared to the gripper that cannot vary its gripping length.

SMA based soft actuator was selected in this work due to its advantages of compact configuration and its large composition of elastomeric polymers being able to easily integrate with other functional components, such as variable stiffness mechanism in this design. The principle used of stiffness variation is based on thermally activated phase-changing materials. The merit of this principle is that the

mechanism can be designed in a compact configuration, which can be easily integrated into other soft actuators or structures providing the ability of changeable stiffness into applications. Besides, the stiffness variation can be easily tailored by modifying the geometrical parameters or the volume of the embedded phase-changing materials. However, the stiffness variation from the low state to the high state requires a long time because of the slow heat dissipation led by the low thermal conductivity of the polymeric matrix. For future works, the stiffness variation performance should be improved by changing and optimizing the designs to increase the rate of heat dissipation. Moreover, different principles of variable stiffness along with different types of actuation methods can be applied to soft grippers with more advanced compliance and adaptability.

Author Disclosure Statement

No competing financial interests exist.

Funding Information

This work was supported by the National Research Foundation of Korea (NRF) grant funded by the Korea government (MSIT) (2019R1F1A1062619), a grant to Bio-Mimetic Robot Research Center funded by Defense Acquisition Program Administration and by Agency for Defense Development (UD190018ID), and the research fund of Hanyang University (HY-2019).

Supplementary Material

Supplementary Table S1
Supplementary Figure S1
Supplementary Figure S2
Supplementary Movie S1

References

1. Manti M, Cacucciolo V, Cianchetti M. Stiffening in soft robotics: A review of the state of the art. IEEE Robot Autom Mag 2016;23:93–106.
2. Laschi C, Mazzolai B, Cianchetti M. Soft robotics: technologies and systems pushing the boundaries of robot abilities. Sci Robot 2016;3690:eaah3690.
3. Rus D, Tolley MT. Design, fabrication and control of soft robots. Nature 2015;521:467–475.
4. Laschi C, Cianchetti M. Soft robotics: new perspectives for robot bodyware and control. Front Bioeng Biotechnol 2014;2:3.
5. Wang W, Rodrigue H, Kim H-I, *et al*. Soft composite hinge actuator and application to compliant robotic gripper. Compos Part B Eng 2016;98:397–405.
6. Rodrigue H, Wang W, Kim D-R, *et al*. Curved shape memory alloy-based soft actuators and application to soft gripper. Compos Struct 2017;176:398–406.
7. Shian S, Bertoldi K, Clarke DR. Dielectric elastomer based ''grippers'' for soft robotics. Adv Mater 2015;27:6814–6819.
8. Shintake J, Rosset S, Schubert B, *et al*. Versatile soft grippers with intrinsic electroadhesion based on multifunctional polymer actuators. Adv Mater 2016;28:231–238.
9. Deimel R, Eppner C, Álvarez-Ruiz J, *et al*. Exploitation of environmental constraints in human and robotic grasping. Springer Tracts Adv Robot 2016;114:393–409.
10. Yang D, Mosadegh B, Ainla A, *et al*. Buckling of elastomeric beams enables actuation of soft machines. Adv Mater 2015;27:6323–6327.
11. Yang Y, Chen Y, Li Y, *et al*. Bioinspired robotic fingers based on pneumatic actuator and 3D printing of smart material. Soft Robot 2017;4:147–162.
12. Manti M, Hassan T, Passetti G, *et al*. A Bioinspired soft robotic gripper for adaptable and effective grasping. Soft Robot 2015;2:107–116.
13. Odhner LU, Jentoft LP, Claffee MR, *et al*. a compliant, underactuated hand for robust manipulation. Int J Rob Res 2014;33:736–752.
14. Wang W, Ahn S. Shape memory alloy-based soft gripper with variable stiffness for compliant and effective grasping. Soft Robot 2017;4:1–13.
15. Carpi F, Frediani G, Gerboni C, *et al*. Enabling variable-stiffness hand rehabilitation orthoses with dielectric elastomer transducers. Med Eng Phys 2014;36:205–211.
16. Shan Y, Philen M, Lotfi A, *et al*. Variable Stiffness structures utilizing fluidic flexible matrix composites. J IntellMater Syst Struct 2009;20:443–456.
17. Calisti M, Giorelli M, Levy G, *et al*. An octopus-bioinspired solution to movement and manipulation for soft robots. Bioinspir Biomim 2011;6:036002.
18. Park YJ, Huh TM, Park D, *et al*. Design of a variable-stiffness flapping mechanism for maximizing the thrust of a bio-inspired underwater robot. Bioinspir Biomim 2014;9:036002.
19. Majidi C, Wood RJ. Tunable elastic stiffness with microconfined magnetorheological domains at low magnetic field. Appl Phys Lett 2010;97:164104.
20. Cao C, Zhao X. Tunable stiffness of electrorheological elastomers by designing mesostructures. Appl Phys Lett 2013;103:4–8.
21. Brown E, Rodenberg N, Amend J, *et al*. Universal robotic gripper based on the jamming of granular material. Proc. Natl Acad Sci U S A 2010;107:18809–18814.
22. Narang YS, Vlassak JJ, Howe RD. Mechanically versatile soft machines through laminar jamming. Adv Funct Mater 2018;28:1707136.
23. Cavallo A, Brancadoro M, Tognarelli S, *et al*. A soft retraction system for surgery based on ferromagnetic materials and granular jamming. Soft Robot 2018;6:161–173.
24. Wang W, Rodrigue H, Ahn S-H. Smart soft composite actuator with shape retention capability using embedded fusible alloy structures. Compos Part B Eng 2015;78:507–514.
25. Wang W, Li C, Cho M, *et al*. Soft tendril-inspired grippers: shape morphing of programmable polymer–paper bilayer composites. ACS Appl Mater Interfaces 2018;10:10419–10427.
26. McEvoy MA, Correll N. Shape-changing materials using variable stiffness and distributed control. Soft Robot 2018;5:737–747.
27. Wang W, Rodrigue H, Ahn S-H. Deployable soft composite structures. Sci Rep 2016;6:20869.
28. Rich S, Jang S-H, Park Y-L, *et al*. Liquid metal-conductive thermoplastic elastomer integration for low-voltage stiffness tuning. Adv Mater Technol 2017;2:1700179.
29. Yang Y, Chen Y, Li Y, *et al*. Novel variable-stiffness robotic fingers with built-in position feedback. Soft Robot 2017;4:338–352.
30. She Y, Li C, Cleary J, *et al*. Design and fabrication of a soft robotic hand with embedded actuators and sensors. J Mech Robot 2015;7:021007.

31. Hager MD, Bode S, Weber C, *et al*. Shape memory polymers: past, present and future developments. Prog Polym Sci 2015;49–50:3–33.
32. Wang W, Li C, Rodrigue H, *et al*. Kirigami/origami-based soft deployable reflector for optical beam steering. Adv Funct Mater 2017;27:1604214.
33. Wang W, Kim N-G, Rodrigue H, *et al*. Modular assembly of soft deployable structures and robots. Mater Horiz 2017; 4:367–376.
34. Wang W, Lee J-Y, Rodrigue H, *et al*. Locomotion of inchworm-inspired robot made of smart soft composite (SSC). Bioinspir Biomim 2014;9:046006.
35. Villanueva aa, Joshi KB, Blottman JB, *et al*. A bio-inspired shape memory alloy composite (BISMAC) actuator. Smart Mater Struct 2010;19:025013.
36. Ghosh P, Rao A, Srinivasa AR. Design of multi-state and smart-bias components using shape memory alloy and shape memory polymer composites. Mater Des 2013;44: 164–171.
37. Ratna D, Karger-Kocsis J. Recent advances in shape memory polymers and composites: a review. J Mater Sci 2008;43:254–269.
38. Brinson LC. One-dimensional constitutive behavior of shape memory alloys: thermomechanical derivation with non-constant material functions and redefined martensite internal variable. J Intell Mater Syst Struct 1993;4:229–242.
39. Elahinia MH, Ahmadian M. An enhanced SMA phenomenological model: I. The shortcomings of the existing models. Smart Mater Struct 2005;14:1297–1308.
40. Engeberg ED, Dilibal S, Vatani M, *et al*. Anthropomorphic finger antagonistically actuated by SMA plates. Bioinspir Biomim 2015;10:056002.

Address correspondence to:
Wei Wang
Department of Mechanical Engineering
Hanyang University
Wangsimni-ro 222
Seongdong-gu
Seoul 04763
Republic of Korea

E-mail: hitwangw@gmail.com; davidwang@hanyang.ac.kr

Sung-Hoon Ahn
Department of Mechanical and Aerospace Engineering
Seoul National University
Gwanak-ro 1
Gwanak-gu
Seoul 08826
Republic of Korea

E-mail: ahnsh@snu.ac.kr